

ULRR

Simultaneous measurement of displacement and temperature based on a balloon-shaped bent SMF structure incorporating an LPG

Item Type	Article
Authors	Tian, Ke;Farrell, Gerald;Yang, Wenlei;Wang, Xianfan;Lewis, Elfed;Wang, Pengfei
Citation	Journal of Lightwave Technology;36, pp. 4960-4966
Publisher	IEEE Computer Society
Download date	2026-06-14 01:30:45
Item License	https://creativecommons.org/licenses/by-nc-sa/1.0/
Link to Item	https://hdl.handle.net/10344/8942

Simultaneous Measurement of Displacement and Temperature Based on Balloon-Shaped Bent SMF Structure Incorporating an LPG

Ke Tian, Gerald Farrell, Wenlei Yang, Xianfan Wang, Elfed Lewis, *Senior Member, IEEE*, and Pengfei Wang

Abstract—A novel optical fibre sensor based on a balloon-shaped bent single-mode (BSBS) fibre structure incorporating a long-period grating (LPG) for simultaneous measurement of displacement and temperature is described and experimentally demonstrated. The sensor is fabricated by splicing a BSBS fibre structure formed Mach-Zehnder interferometer (MZI) with an LPG. Due to the interference dip which is formed by the BSBS fibre structure is sensitive to external displacement and temperature variation, while that formed by LPG only depends on temperature, displacement and temperature therefore can be unambiguously and simultaneously measured by this sensor. Experimental results show that this sensor offers a high displacement sensitivity of $-306 \text{ pm}/\mu\text{m}$ over the displacement range of $0\text{--}80 \mu\text{m}$ and a temperature sensitivity of $42.9 \text{ pm}/^\circ\text{C}$ over the temperature range of $20\text{--}45 \text{ }^\circ\text{C}$. Based on its high measurement sensitivities, low cost and good repeatability, the sensor of this investigation could be a realistic candidate for applications where displacement and temperature need to be measured simultaneously.

Index Terms—Mach-Zehnder interferometer, long-period grating, displacement measurement, temperature measurement.

This work was supported by the Key Program for International S&T Cooperation Projects of China under grant 2016YFE0126500, the National Natural Science Foundation of China (NSFC) under grant 61575050, the Key Program for Natural Science Foundation of Heilongjiang Province of China under grant ZD2016012, the Open Fund of the State Key Laboratory on Integrated Optoelectronics under grant IOSKL2016KF03, the 111 project to the Harbin Engineering University under grant B13015, and the Ph. D Student Research and Innovation Fund of the Fundamental Research Funds for the Central Universities (HEUGIP201820). (*Corresponding author: Pengfei Wang*)

P. Wang is with Key Laboratory of In-fiber Integrated Optics of Ministry of Education, College of Science, Harbin Engineering University, Harbin 150001, China. Key Laboratory of Optoelectronic Devices and Systems of Ministry of Education and Guangdong Province, College of Optoelectronic Engineering, Shenzhen University, Shenzhen, 518060, China (email: pengfei.wang@dit.ie). K. Tian, G. Farrell, W. Yang and X Wang are with the Key Laboratory of In-fiber Integrated Optics of Ministry of Education, College of Science, Harbin Engineering University, Harbin 150001, China (e-mail: ketian@hrbeu.edu.cn; gerald.farrell@dit.ie; yangwenlei@hrbeu.edu.cn; heuwangfan@hrbeu.edu.cn). P. Wang and G. Farrell are also with the Photonics Research Centre, Dublin Institute of Technology, Kevin Street, Dublin 8, Ireland (email: pengfei.wang@dit.ie; gerald.farrell@dit.ie).

E. Lewis is with the Optical Fibre Sensors Research Centre, Department of Electronic and Computer Engineering, University of Limerick, Limerick, Ireland (email: Elfed.lewis@ul.ie).

I. INTRODUCTION

Displacement measurement plays an important role in current industrial manufacturing, and high-accuracy displacement sensors are frequently required in many specialized application areas including astronautics, microimaging and structural health monitoring (SHM). To meet these requirements, different types of displacement sensors have been developed in recent years. Compared with traditional electronic displacement sensors, optical fibre based micro-displacement sensors have attracted significant attention owing to their unique advantages of compact structure, their potential for remote operation and immunity to external electromagnetic interference. To date, a number of optical fibre micro-displacement sensors have been developed based on fibre Bragg gratings (FBG) [1-3], long period gratings (LPG) [4], multimode interference (MMI) [5, 6] and various fibre interferometers including Mach-Zehnder interferometers (MZI) [7, 8], a Fabry-Perot interferometer (FPI) [9], a Sagnac interferometer [10] and other modal interferometers [11].

Among these structures, optical fibre interferometric displacement sensors offer higher resolution, better stability and wider dynamic range than other sensor types, but their disadvantages include fragility, complex pre-processing that often requires access to expensive infrastructure such as femtosecond lasers or highly accurate tapering facilities, all of which restricts their development in practical applications. Therefore, a fibre interferometer structure based on a simple fabrication process would be of significant value. Recently, an interferometer formed using bent SMF has attracted significant research attention because it is an inherently simple structure and is thus easy to fabricate. However, in a previous study, it has been demonstrated that it has a relatively high temperature dependence of $418 \text{ pm}/^\circ\text{C}$ [12]. Therefore, whilst it may be considered a desirable sensor candidate for temperature measurement, as a displacement sensor it would possess a particularly undesirable temperature cross-sensitivity. To overcome the temperature induced cross-sensitivity, simultaneous measurement of a target and temperature is a commonly used solution. For example in Ref. [12], the simultaneous measurement of RI and temperature could be realized by interrogating the wavelength shift and intensity variation of the same interference dip, however the measurement accuracy and

stability of the sensor system is unstable because the wavelength and the intensity of the selected interference dip are mostly depend on the changes of RI and temperature. As well-known traditionally FBGs and LPGs are often used as part of a sensing scheme to achieve the goal of simultaneous measurement for many parameters, e.g. refractive index (RI) [13, 14], strain [15], curvature[16], humidity [17], displacement [18], etc.

In this article, a novel optical fibre sensor based on a BSBS fibre structure incorporating an LPG for simultaneous displacement and temperature measurement is described. The schematic configuration of the sensor is shown in Fig. 1. The BSBS fibre structure is simply fabricated by bending a SMF into a balloon shape using a section of capillary tube, and the complete sensor structure is realized by splicing it to an LPG. The BSBS fibre structure is used to measure external displacement and the LPG is used to generate a reference spectral dip to achieve the goal of simultaneous measurement of temperature and thus providing a means of temperature compensation. The experimental results demonstrate that displacement and temperature can be unambiguously measured by this sensor, and maximum measurement sensitivities of -306 pm/ μm and 42.9 pm/ $^{\circ}\text{C}$ have achieved experimentally.

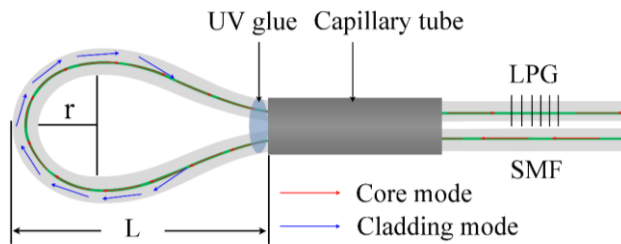


Fig. 1. Schematic diagram of the proposed sensor based on a BSBS fibre structure incorporating an LPG.

II. DEVICE FABRICATION AND MEASUREMENT PRINCIPLE

A. Balloon-Shaped Bent SMF (BSBS) Structure

Fig. 1 illustrates the schematic diagram of the BSBS fibre structure based Mach-Zehnder Interferometer (MZI) configuration. The bending radius and the length of the balloon-shaped section are defined as r and L respectively. The light from the source initially propagates along the input straight section of the SMF as a core mode. When the light arrives at the balloon-shaped section, due to the bend in the waveguide, a portion of the light is coupled into the cladding at which point it excites the cladding modes. These excited cladding modes propagate within the SMF cladding, and following propagation through the bend region, a portion of the cladding mode energy is re-coupled back into the SMF core. Interference between the cladding modes and the mode propagating in the core occurs and thus an MZI is formed due the existence of differences in effective refractive indices (RIs) of the core and cladding and the optical paths differences experienced by the light signals propagating in the core mode and the cladding modes. In the case of a typical two-mode MZI, the output intensity can be expressed as follows [19]:

$$I_{out} = I_{co} + I_{cl} + 2\sqrt{I_{co}I_{cl}} \cos(\varphi + \varphi_0) \quad (1)$$

where I_{co} and I_{cl} is the intensity of the core mode and the cladding mode, respectively, and φ_0 is the initial phase. φ is the phase difference between the core mode and the cladding mode which can be expressed as [20]:

$$\varphi = \frac{2\pi L_{eff}}{\lambda} \Delta n_{eff} \quad (2)$$

where L_{eff} is the effective bent length, λ is the free space wavelength and $\Delta n_{eff} = n_{coeff} - n_{clcoeff}$ is the effective RI difference between the core and cladding modes, where n_{coeff} and $n_{clcoeff}$ are the core and cladding effective RI values. When the phase difference meets the condition of $\varphi = (2m+1)\pi$, $m=0, 1, 2, \dots$, an interference dip appears at specific wavelengths [21]:

$$\lambda_m = \frac{2L_{eff} \Delta n_{eff}}{2m+1} \quad (3)$$

The free spectral range (FSR) of the transmission spectrum can be approximately calculated using the following expression [22]:

$$FSR = \frac{\lambda_m^2}{L_{eff} \Delta n_{eff}} \quad (4)$$

It is clear from Eq. (4) that the FSR of the transmission spectrum decrease as the effective bending length L_{eff} increases. It is worth noting that the effective bending length L_{eff} is not simply the length of the bent section but is an effective length that allows the transmission of the excited cladding mode. In general, a larger bending angle allows light to be coupled into the cladding earlier in its transmission process and therefore produce a larger transmission length for the excited cladding mode, which means in a curved structure, a smaller bending radius r can achieve a larger L_{eff} .

When the external displacement or temperature varies, the value of Δn_{eff} and L_{eff} also changes which results in the variation of the transmission spectrum according to Eq. (3). Therefore, in principle the MZI formed by the BSBS fibre structure can be used to perform displacement and temperature measurement.

Based on the above theoretical analysis, the initial transmission spectrum (in the range 1500 nm to 1600 nm) of a BSBS fibre structure with different bending radii was observed experimentally. When the bending radius of the SMF was greater than 7 mm, no interference pattern appears within the wavelength range since little or no light energy in the fibre core is coupled into the cladding. The bending radius was then decreased from 7 mm to 3.75 mm, and the measured results are shown in Fig. 2. It can be observed from Fig. 2 that with decreasing the bending radius, the intensity loss of the transmission spectrum increases because more light is coupled into the fibre cladding. When the bending radius reaches a value between 7 mm and 6 mm, interference fringes appeared, but no suitable interference dip was detected. With a further decrease of the bending radius to 4.25 mm, an available interference dip appeared with a relatively large extinction ratio (more than 15 dB). As the bending radius was further decreased to 3.75 mm, more interference dips were detected which means that the FSR of the transmission spectrum decreases. Moreover, the extinction ratio of these interference dips

also decreases. If the bending radius continues to decrease, excess light is coupled into the cladding and can even leak out from the cladding resulting in a large signal loss. Ultimately, these initial exploratory experiments determined that an appropriate bending radius to form an effective MZI should lie in the region around 4.25 mm.

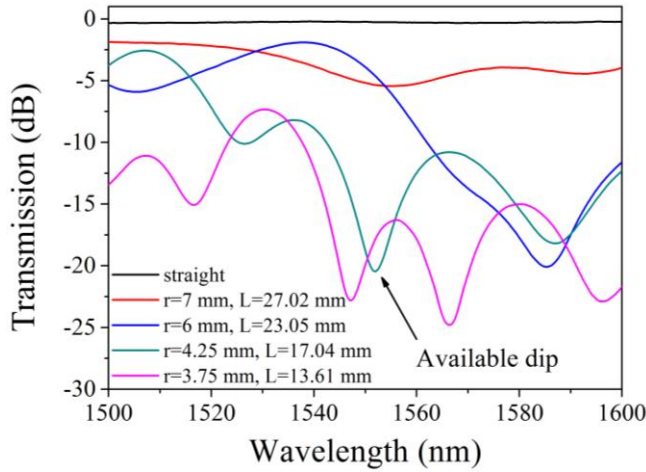


Fig. 2. Transmission spectrum of the BSBS fibre structure with different bending radii.

The fabrication of the BSBS fibre structure is a relatively simple process. Initially a single-mode fibre (SMF-28, Corning) was stripped of its coating over a suitable length, and both ends of it were inserted into a capillary tube for which the length and inner diameter are 1.5 cm and 600 μm , respectively. By moving this silica capillary tube along the fibre, the bending radius of the balloon-shaped section can be flexibly adjusted. After the optimum bending radius was determined, ultraviolet (UV) glue was used to immobilize the BSBS fibre structure. Two bend parameter values were measured including the bending radius r value of 4.28 mm and the length of the balloon-shaped section L of 17.11 mm (as defined previously in Fig. 1). The transmission spectrum of the obtained sample was measured and is depicted in Fig. 3 (red line). As shown in Fig. 3, a desired dip with a central wavelength located at 1547 nm was chosen to perform the sensing measurement since it has a relatively good wavelength location and extinction ratio (18.13 dB).

B. LPG

LPGs normally have a grating period in the range of 100 μm to 1 mm and are different from FBGs in that the optical interference in an LPG occurs between in the forward-propagating core mode and the forward-propagating cladding modes. The resonance wavelength which meets the phase matching condition can be expressed as [23]:

$$\lambda_{res} = (n_{coeff} - n_{clEFF})\Lambda \quad (5)$$

where λ_{res} is the resonance wavelength, and Λ is the grating period.

When the surrounding temperature is changed, due to the thermo-optic and thermal expansion effect of the optical fibre, the values of effective RI of the core mode and cladding mode as well as the grating period Λ change. The resulting temperature sensitivity of LPG can be further expressed as [24]:

$$\frac{d\lambda_{res}}{dT} = \frac{d\lambda_{res}}{d(\Delta n_{eff})} \left(\frac{dn_{coeff}}{dT} - \frac{dn_{clEFF}}{dT} \right) + \Lambda \frac{d\lambda_{res}}{d\Lambda} \frac{1}{L_i} \frac{dL_i}{dT} \quad (6)$$

where T is the temperature and L_i is the length of the LPG.

The LPG used experimentally was a conventional LPG with a period and period number equal to 611 μm and 40, respectively. The transmission spectrum of the LPG was measured and shown in Fig. 3 (black line). It is clear that an interference dip attributed to the LPG appears over the wavelength range of 1515 to 1600 nm and its central wavelength is located at 1583.95 nm.

Following preparation of these two structures, the complete sensor structure was realized by simply splicing these two structures together. The transmission spectrum of the composite structure was measured and shown in Fig. 3 (blue line). From Fig. 3, we can see that the apparent dip location of the bend MZI dip and the LPG dip exhibit tiny shifts, which is due to the superposition of transmission characteristics (red and black lines). The final central wavelength of the bend MZI dip and the LPG dip are located at 1546.2 nm and 1585.6 nm, respectively.

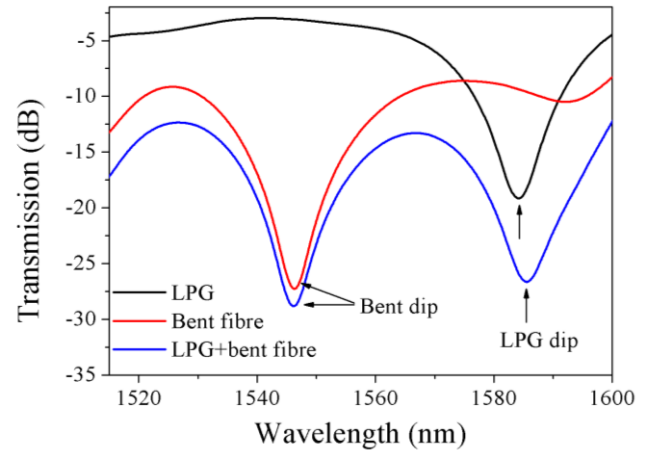


Fig. 3. The transmission spectrum of the single BSBS fibre structure, the single LPG and the composite structure.

Based on the above discussions, when the surrounding temperature and displacement change, the resulting wavelength shift of the bend MZI dip $\Delta\lambda_{bent}$ and the LPG dip $\Delta\lambda_{LPG}$ can be expressed as follows:

$$\Delta\lambda_{bent} = K_{T1} \cdot \Delta T + K_{D1} \cdot \Delta D \quad (7)$$

$$\Delta\lambda_{LPG} = K_{T2} \cdot \Delta T + K_{D2} \cdot \Delta D \quad (8)$$

where ΔT and ΔD represent the variation of temperature and displacement, K_{T1} and K_{D1} are the sensitivities of the bend MZI dip response to temperature and displacement, respectively, and K_{T2} and K_{D2} are the sensitivities of the LPG dip response to temperature and displacement, respectively.

In the principle for the measurement configuration which is illustrated in Fig. 4, the external displacement change is just applied on the BSBS fibre structure, hence it is possible to predict that the LPG dip is independent of displacement which means the K_{D2} should be equal to 0. The following experiments are performed to demonstrate this fact and determine the rest of coefficients in Eq. (7) and (8). Once these coefficients are

determined, a demodulation matrix can be established to achieve the goal of simultaneous measurement of displacement and temperature.

III. EXPERIMENTS AND DISCUSSION

A. Displacement Measurement

The experimental setup for displacement measurement is shown in Fig. 4. The sample was placed and fixed on a lifting platform of adjustable height. A one-dimensional manually tuned translation stage with a 10 μm displacement resolution was used to accurately change the axial displacement which was applied on the balloon-shaped section. A supercontinuum light source (SCS, YSL SC-series, China) was connected to the input SMF of the sensor, and the output transmission spectrum was recorded using a high-resolution (20 pm) optical spectrum analyzer (OSA, YOKOGAWA AQ6370D, Japan).

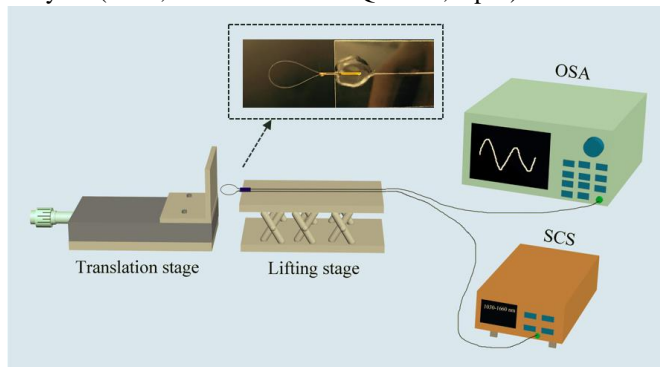


Fig. 4. Schematic diagram of the experimental setup for displacement measurement.

The transmission spectrum evolution of the proposed sensor when subjected to a displacement range from 0 to 80 μm with a step of 10 μm is presented in Fig. 5 (a). In order to test the repeatability of this sensor, a reversed measurement cycle was carried out in which the displacement is decreased from 80 μm back to 0, and the result is presented in Fig. 5 (b). As shown in Fig. 5 (a), of the two separate interference dips exhibit different evolution features when the displacement was changed. The bend MZI dip exhibits a clear blue shift while the LPG dip has no wavelength shift as the displacement is increased from 0 to 80 μm . When the displacement is decreased from 80 μm to 0, the bend MZI dip is opposite to case where the displacement increases, which is clearly depicted in Fig. 5 (b).

From the above experimental results, it was demonstrated that the LPG dip is independent of displacement, hence its displacement sensitivity can be denoted as 0. However, in the case of the bend MZI dip, the displacement variation strongly influences the location of its central wavelength. The resulting wavelength shift of the bend MZI dip with displacement increasing and decreasing were linearly fitted against the displacement value in Fig. 6. It can be seen that both of the fitting curves exhibit high linear regression coefficient values (R^2) of 0.9977 and 0.9958, and the displacement sensitivities as the displacement increases and decreases were determined to be -306 pm/ μm and -308 pm/ μm , respectively. Based on the fitting curves and sensitivities

determined from Fig. 6, it is also demonstrated that the bend MZI dip offers good repeatability for displacement measurement on account of the very small differences between the results for the displacement increase and decrease cases.

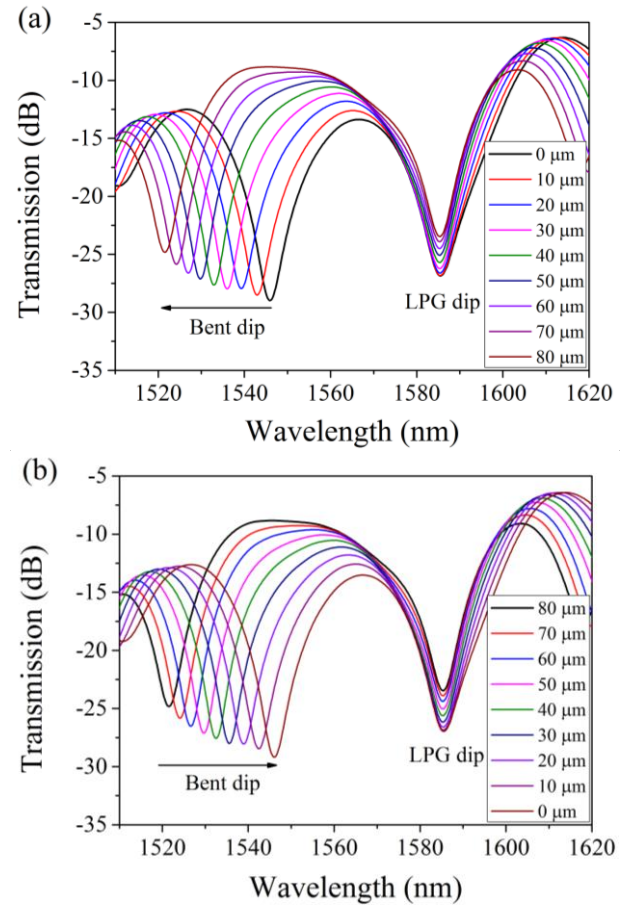


Fig. 5. The transmission spectrum evolution as displacement is changed (a) displacement increases; (b) displacement decreases.

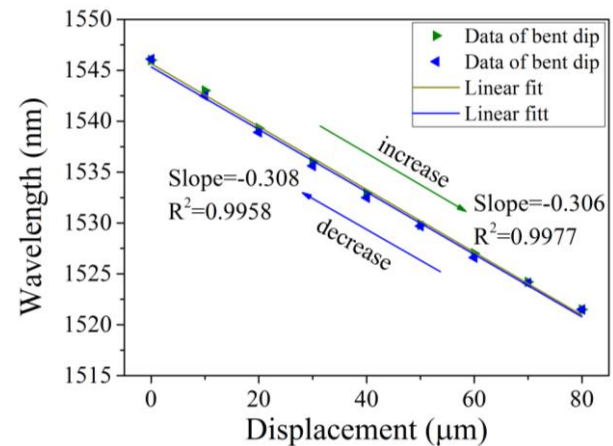


Fig. 6. Linear fitting curves of bend MZI dip wavelength shifts against displacement variation.

B. Temperature Measurement

To characterize the temperature response of this sensor, the sample was placed inside a climate chamber (ESPEC SH-222, Japan), in which the temperature can be accurately controlled, and the real-time temperature value is shown on its external

display panel. The previously mentioned SCS and OSA were used as the light source and detector respectively. The corresponding experimental setup is shown in Fig.7.

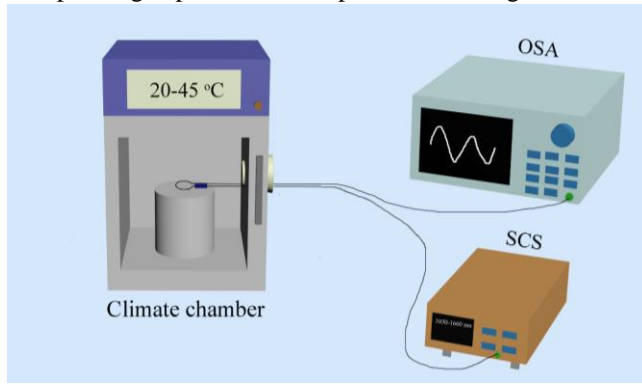


Fig.7. Schematic diagram of the experiment setup for temperature measurement.

The temperature of the climate chamber was changed from 20 °C to 45 °C with a step of 5 °C. The corresponding spectral evolution and the fitting results of the bend MZI dip and the LPG dip are shown in Fig. 8 (a) and (b), respectively. From the insert pictures in Fig. 8 (a) and (b), as the temperature increased in the range of 20 °C to 45 °C, the bend MZI dip and the LPG dip moved toward a longer wavelength. Both of these dips exhibit a highly linear response to temperature ($R^2=0.9885$ for the bend

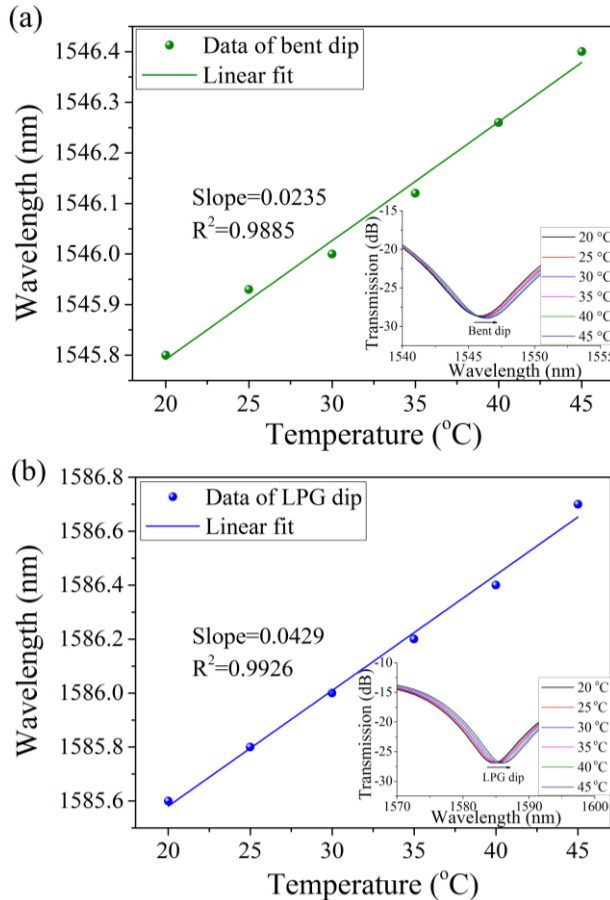


Fig.8. Wavelength shift against surrounding temperature variation (a) linear fitting result of the bend MZI dip and the corresponding spectral evolution inserts in the picture; (b) linear fitting result of LPG dip and the corresponding spectral evolution inserts in the picture.

MZI dip, $R^2=0.9926$ for the LPG dip), and the linear fitting results show that the temperature sensitivities of the bend MZI dip and the LPG dip correspond to 23.5 pm/°C and 42.9 pm/°C, respectively.

The above experimental results indicate that the bend MZI dip is sensitive to external displacement and temperature variation, while that the LPG dip is independent of displacement which enables it to be used for temperature compensation and achieves the function of simultaneous displacement and temperature measurement. Based on the obtained sensitivity coefficients and Eq. (7) and (8), a demodulation matrix was established to determine the value of external displacement and surrounding temperature, which is expressed as:

$$\begin{bmatrix} \Delta T \\ \Delta D \end{bmatrix} = \begin{bmatrix} 23.5 \text{ pm}/^\circ\text{C} & -306 \text{ pm}/\mu\text{m} \\ 42.9 \text{ pm}/^\circ\text{C} & 0 \end{bmatrix}^{-1} \begin{bmatrix} \Delta \lambda_{\text{bent}} \\ \Delta \lambda_{\text{LPG}} \end{bmatrix} \quad (9)$$

Furthermore, given the 20 pm resolution of the OSA used in the experiment, the displacement and temperature measurement resolution of this sensor system were calculated to be 0.07 μm and 0.47 °C, respectively, which are acceptable in practical applications.

Table 1 shows a comparison of the sensing performance for displacement and temperature between the sensor described in this investigation and the other optical fibre sensors cited in this article. From Table 1, it is clear that the achieved displacement and temperature sensitivities of the sensor in this investigation compare favorably with all of the cited sensors. In addition to the direct advantage of high sensitivity, this proposed sensor also achieves the goal of simultaneous measurement, which can eliminate the temperature induced cross-sensitivity during practical measurements. Consequently, the low cost, high sensitivity sensor described in this investigation can be a realistic candidate for use in accurate displacement and temperature measurement fields.

TABLE I
COMPARISON OF THE PERFORMANCE OF DIFFERENT SENSORS FOR
DISPLACEMENT AND TEMPERATURE MEASUREMENT

Measurement configuration	Displacement sensitivity (pm/ μm)	Temperature sensitivity (pm/°C)	Simultaneous measurement	Ref.
Tilted FBG	121	-	No	[1]
FBG	0.567	-	No	[2]
FBG	0.0643	16.9	Yes	[3]
LPG	220	-	No	[4]
MMI	25	-	No	[5]
MMI	5.89	11.6	Yes	[6]
MZI	227	-	No	[7]
MZI	-1.89 dB/ μm	0.02	No	[8]
FPI	-	-	No	[9]
Sagnac interferometer	-	-	No	[10]
Modal interferometer	-15.35	4.93	Yes	[11]
Tapered fibre with FBG	0.11 dB/ μm	9.7	Yes	[18]
Bent fibre with LPG	-306	42.9	Yes	This work

IV. CONCLUSION

A novel fiber-optic sensor based on a balloon-shaped bent single-mode (BSBS) fibre structure incorporating an LPG for simultaneous measurement of displacement and temperature has been described. The sensor was simply realized by splicing a BSBS fibre with an LPG. Since the spectral dip of the BSBS fibre structure is sensitive to both external displacement and temperature variation, the LPG was introduced to generate a reference dip to facilitate unambiguous displacement and temperature measurement. The experimental results show that this sensor provides a high displacement sensitivity of $-306 \text{ pm}/\mu\text{m}$ over the displacement range of $0\text{--}80 \mu\text{m}$ and a temperature sensitivity of $42.9 \text{ pm}/^\circ\text{C}$ over the temperature range of $20\text{--}45 \text{ }^\circ\text{C}$. Based on the sensitivity coefficients obtained for these two kinds of dips, a demodulation matrix was successfully established.

REFERENCES

- [1] Q. Jiang and D. Hu, "Microdisplacement sensor based on tilted fiber Bragg grating transversal load effect," *IEEE Sensors Journal*, vol. 11, pp. 1776-1779, 2011.
- [2] S. Tao, X. Dong, and B. Lai, "Temperature-insensitive fiber Bragg grating displacement sensor based on a thin-wall ring," *Optics Communications*, vol. 372, pp. 44-48, 2016.
- [3] Y. Yu, H. Tam, W. Chung, and M. S. Demokan, "Fiber Bragg grating sensor for simultaneous measurement of displacement and temperature," *Optics Letters*, vol. 25, pp. 1141-1143, 2000.
- [4] L. Qi, C.-L. Zhao, Y. Wang, J. Kang, Z. Zhang, and S. Jin, "Compact micro-displacement sensor with high sensitivity based on a long-period fiber grating with an air-cavity," *Optics Express*, vol. 21, pp. 3193-3200, 2013.
- [5] J. Antonio-Lopez, P. LiKamWa, J. Sanchez-Mondragon, and D. May-Arrioja, "All-fiber multimode interference micro-displacement sensor," *Measurement Science and Technology*, vol. 24, pp. 055104, 2013.
- [6] Q. Wu, A. M. Hatta, P. Wang, Y. Semenova, and G. Farrell, "Use of a Bent Single SMS Fiber Structure for Simultaneous Measurement of Displacement and Temperature Sensing," *IEEE Photonics Technology Letters*, vol. 23, pp. 130-132, 2011.
- [7] J. Chen, J. Zhou, and Z. Jia, "High-sensitivity displacement sensor based on a bent fiber Mach-Zehnder interferometer," *IEEE Photonics Technology Letters*, vol. 25, pp. 2354-2357, 2013.
- [8] C.-Y. Shen, J.-L. Chu, Y.-F. Lu, D.-B. Chen, C. Zhong, Y. Li, *et al.*, "High sensitive micro-displacement sensor based on MZ interferometer by a bowknot type taper," *IEEE Photonics Technology Letters*, vol. 26, pp. 62-65, 2014.
- [9] X. Zhou and Q. Yu, "Wide-range displacement sensor based on fiber-optic Fabry-Perot interferometer for subnanometer measurement," *IEEE Sensors Journal*, vol. 11, pp. 1602-1606, 2011.
- [10] M. Bravo, A. Pinto, M. Lopez-Amo, J. Kobelke, and K. Schuster, "High precision micro-displacement fiber sensor through a suspended-core Sagnac interferometer," *Optics Letters*, vol. 37, pp. 202-204, 2012.
- [11] J. Wu, Y. Miao, B. Song, W. Lin, K. Zhang, H. Zhang, *et al.*, "Simultaneous measurement of displacement and temperature based on thin-core fiber modal interferometer," *Optics Communications*, vol. 340, pp. 136-140, 2015.
- [12] X. Liu, Y. Zhao, R.-Q. Lv, and Q. Wang, "High sensitivity balloon-like interferometer for refractive index and temperature measurement," *IEEE Photonics Technology Letters*, vol. 28, pp. 1485-1488, 2016.
- [13] Q. Yao, H. Meng, W. Wang, H. Xue, R. Xiong, B. Huang, *et al.*, "Simultaneous measurement of refractive index and temperature based on a core-offset Mach-Zehnder interferometer combined with a fiber Bragg grating," *Sensors and Actuators A: Physical*, vol. 209, pp. 73-77, 2014.
- [14] D. W. Kim, F. Shen, X. Chen, and A. Wang, "Simultaneous measurement of refractive index and temperature based on a reflection-mode long-period grating and an intrinsic Fabry-Perot interferometer sensor," *Optics Letters*, vol. 30, pp. 3000-3002, 2005.
- [15] L. Wang, W. Zhang, B. Wang, L. Chen, Z. Bai, S. Gao, *et al.*, "Simultaneous strain and temperature measurement by cascading few-mode fiber and single-mode fiber long-period fiber gratings," *Applied Optics*, vol. 53, pp. 7045-7049, 2014.
- [16] Y. Zhou, W. Zhou, C. C. Chan, W. C. Wong, L.-Y. Shao, J. Cheng, *et al.*, "Simultaneous measurement of curvature and temperature based on PCF-based interferometer and fiber Bragg grating," *Optics Communications*, vol. 284, pp. 5669-5672, 2011.
- [17] F. J. Arregui, I. R. Matías, K. L. Cooper, and R. O. Claus, "Simultaneous measurement of humidity and temperature by combining a reflective intensity-based optical fiber sensor and a fiber Bragg grating," *IEEE Sensors Journal*, vol. 2, pp. 482-487, 2002.
- [18] C. Ji, C.-L. Zhao, J. Kang, X. Dong, and S. Jin, "Multiplex and simultaneous measurement of displacement and temperature using tapered fiber and fiber Bragg grating," *Review of Scientific Instruments*, vol. 83, p. 053109, 2012.
- [19] H. Y. Choi, M. J. Kim, and B. H. Lee, "All-fiber Mach-Zehnder type interferometers formed in photonic crystal fiber," *Optics Express*, vol. 15, pp. 5711-5720, 2007.
- [20] Z. Tian, S. S.-H. Yam, J. Barnes, W. Bock, P. Greig, J. M. Fraser, *et al.*, "Refractive index sensing with Mach-Zehnder interferometer based on concatenating two single-mode fiber tapers," *IEEE Photonics Technology Letters*, vol. 20, pp. 626-628, 2008.
- [21] P. Chen, X. Shu, and K. Sugden, "Ultra-compact all-in-fiber-core Mach-Zehnder interferometer," *Optics Letters*, vol. 42, pp. 4059-4062, 2017.
- [22] L. V. Nguyen, D. Hwang, S. Moon, D. S. Moon, and Y. Chung, "High temperature fiber sensor with high sensitivity based on core diameter mismatch," *Optics Express*, vol. 16, pp. 11369-75, 2008.
- [23] Y.-J. Rao, Y.-P. Wang, Z.-L. Ran, and T. Zhu, "Novel fiber-optic sensors based on long-period fiber gratings written by high-frequency CO₂ laser pulses," *Journal of Lightwave Technology*, vol. 21, pp. 1320, 2003.
- [24] S. W. James and R. P. Tatam, "Optical fibre long-period grating sensors: characteristics and application," *Measurement science and technology*, vol. 14, pp. R49, 2003.